easier than that of the fully occupied Ti layer. It is probable that the stacking faults which occur at a low temperature such as 683 K are due only to the slide between the sandwiches, and the experimental data shown in Fig. 1 should be interpreted appropriately on the basis of the extended model.

Experimental patterns which suggest the occurrence of stacking faults are often observed for the various temperatures and compositions in the Ti–S system. The method of analysis of the structure with stacking faults described above may be effectively used for considering the phase-relation problem in this system.

References

BRINDLEY, G. W. & MÉRING, J. (1948). *Nature (London)*, **161**, 774–775.

MALMROS, G. & THOMAS, J. O. (1977). *J. Appl. Cryst.* **10**, 7–11.

ONODA, M. & KAWADA, I. (1980). *Acta Cryst.* A**36**, 134–139.

ONODA, M. & SAEKI, M. (1980). *Chem. Lett.* pp. 665–666.

SAEKI, M., ONODA, M., KAWADA, I. & NAKAHIRA, M. (1980). *J. Less-Common Met.* In the press.

WARREN, B. E. (1941). *Phys. Rev.* **59**, 693–698.

WARREN, B. E. (1959). *Prog. Met. Phys.* **8**, 147–202.

Acta Cryst. (1980). A**36**, 957–965

Dynamic Deformation and the Debye–Waller Factors for Silicon-Like Crystals

BY JOHN S. REID AND JOHN D. PIRIE

Department of Natural Philosophy, The University, Aberdeen AB9 2UE, Scotland

(*Received* 4 *March* 1980; *accepted* 27 *May* 1980)

Abstract

Calculations are presented of the Debye–Waller factors for silicon, diamond and germanium in the temperature range 1 to 1000 K and for grey tin in the range 1 to 280 K. Values were obtained from the shell model, the adiabatic bond-charge model and the valence force potential model for all four materials. Further values are listed from the fitted Born–von Kármán model for silicon and germanium and from two additional parametrizations of the valence force potential model for silicon. The effect of dynamic deformation on the Debye–Waller factor of silicon and, to a slightly lesser extent, the other three elements, is investigated. The Debye–Waller factor for the shells only in the the shell models is calculated. The effect introduced by dynamic deformation whereby the Debye–Waller B value varies with scattering vector $\mathbf{K}$ is evaluated. Finally, the anisotropic Debye–Waller factor components for the bond charges are calculated for all four elements. It is found that the bond charges in the bond-charge model and the shells in the shell model vibrate substantially less than the main atomic cores. It is concluded that if the models are at all realistic then the effects of dynamic deformation on the Debye–Waller factors of these elements should be seriously considered.

Introduction

Interest in the scattering caused by dynamic deformation of electron distributions has arisen from essentially two different sources. On the one hand detailed investigation into thermal diffuse scattering processes has suggested that some contribution to the X-ray scattering is made by the deformation of the electron distribution during thermal vibration, as, for example, has been discussed by Buyers, Pirie & Smith (1968). On the other hand, very accurate crystallographic structural determinations are reaching the stage with favourable materials that different thermal motions of different parts of the electron distribution associated with one particular atom may be experimentally distinguished. An example of these possibilities has been discussed by Price, Maslen & Mair (1978) in the analysis of data for silicon.

In succeeding sections the aim is to bring the insight generated by thermal diffuse scattering studies to bear on the effect which is of most interest to the structural crystallographer, namely the Debye–Waller factor. Although particular emphasis is placed on providing numerical information for silicon, partly for comparison and partly for their intrinsic interest, additional calculations are presented for diamond, germanium and α-tin.

The dynamical deformation formalism is, essentially, a general parametric description of the influence of dynamically distorting electron distributions on the X-ray scattering. The formalism enables distorting atoms to be treated in a similar way to rigid atoms provided certain terms in the cross section are redefined so that, in effect, additional terms are added to the scattering cross sections. As a consequence, any cross

0567-7394/80/060957-09$01.00

section can be developed with a general set of parameters (β parameters, so called after Born, 1942) without prejudice to the specific nature of the deformation which takes place in a given situation. Once a detailed physical model of the deformation is proposed then this model will generate a subset of the general β parameters with relationships between the members and values determined by the model characteristics.

A preceding paper, Reid (1979) hereinafter referred to as (I), showed how the Debye–Waller factors were affected in the general formalism and considered the particular case of shell-model deformations in the alkali halides. Before discussing the extensions of this approach to silicon and related elements we begin by introducing different dynamical models and calculating the Debye–Waller factors given by these various models.

Lattice-dynamical models and their Debye–Waller factors

One of the main purposes of a lattice-dynamical model is to provide an interpolative scheme to determine anywhere in the Brillouin zone the lattice frequencies and polarization vectors from a necessarily small number of experimental frequency measurements. Two types of model with *no* atomic deformation have been successfully fitted to measured frequency and elastic data, namely the valence force potential models and the simple Born–von Kármán model. Apart from fitting the data well, these models have the additional merit of requiring no Coulomb coefficients and hence can speedily produce eigendata over a very fine mesh of wavevectors covering the entire zone.

The Debye–Waller B values were calculated for silicon for the six-parameter valence force potential models of Singh & Dayal (1970), Solbrig (1971) and Tubino, Piseri & Zerbi (1972) and the Born–von Kármán model of Zdetsis & Wang (1979) by direct evaluation of the expression

$$B = \frac{8\pi^2}{6m}\frac{1}{N}\sum_{\lambda}\left(\frac{E}{\omega^2}\right)_{\lambda}. \qquad (1)$$

This simplification of the general expression (see I) can be used for silicon-type materials because appropriate normal coordinates give eigenvectors

$$\mathscr{E}(2/\lambda) = \mathscr{E}^*(1/\lambda). \qquad (2)$$

[The 2 and 1 for the k values in the eigenvectors $\mathscr{E}(k/\lambda)$ refer to the two different atom sites in the silicon unit cell.] One consequence of this relation is that the eigenvector for each atom site has a magnitude of $1/\sqrt{2}$ regardless of wavevector.

The summation (1) was taken over 3 072 000 frequencies in the Brillouin zone to reduce sampling errors to negligible proportions. The zero-phonon contribution was evaluated analytically, though for this sampling density it typically comes to about 0·5% at room temperature and less at lower temperatures. No estimates for quasiharmonic frequency shifts were included with the variation in temperature.

The B values given by these models are included in Table 1. Since all the valence force potential models

Table 1. *Debye–Waller B values* (Å^2) *for silicon calculated from the lattice-dynamical models referred to in the text*

All the models are good ones with their parameters determined to some extent from lattice frequencies measured by slow-neutron scattering at room temperature. The fourth decimal place is not really significant and is included to assist interpolation.

Temperature (K)	Shell model	Bond charge	VFP Solbrig	VFP Singh	VFP Tubino	BVK
1·0	0·1937	0·1881	0·1825	0·1849	0·1857	0·1863
5·0	0·1937	0·1882	0·1826	0·1850	0·1858	0·1864
10·0	0·1939	0·1883	0·1828	0·1852	0·1860	0·1866
20·0	0·1947	0·1891	0·1835	0·1861	0·1868	0·1874
40·0	0·1999	0·1934	0·1875	0·1907	0·1914	0·1918
60·0	0·2116	0·2030	0·1963	0·2004	0·2012	0·2014
80·0	0·2286	0·2172	0·2093	0·2146	0·2154	0·2157
100·0	0·2491	0·2349	0·2256	0·2321	0·2330	0·2333
150·0	0·3100	0·2882	0·2751	0·2848	0·2860	0·2865
200·0	0·3786	0·3493	0·3321	0·3450	0·3465	0·3472
250·0	0·4514	0·4147	0·3934	0·4095	0·4113	0·4122
295·0	0·5192	0·4758	0·4507	0·4697	0·4718	0·4729
350·0	0·6038	0·5522	0·5225	0·5451	0·5476	0·5489
400·0	0·6819	0·6230	0·5890	0·6148	0·6177	0·6192
500·0	0·8402	0·7665	0·7240	0·7562	0·7599	0·7617
600·0	1·0001	0·9117	0·8608	0·8994	0·9038	0·9060
700·0	1·1610	1·0579	0·9985	1·0436	1·0486	1·0513
800·0	1·3226	1·2047	1·1368	1·1884	1·1942	1·1972
900·0	1·4847	1·3520	1·2756	1·3336	1·3401	1·3435
1000·0	1·6470	1·4996	1·4147	1·4791	1·4864	1·4902

were fitted to similar, though not identical, data sets it is surprising that Solbrig's model should produce significantly different values. In fairness to Solbrig it must be added that he considered his own nine-parameter model to be an improvement over his six-parameter model but we have not investigated this refinement.

A comparison between the models is presented more suitably on a diagram as a plot of the Debye temperature Θ_M. Most of the temperature dependence of B which is common to all the models is taken up by the relation between B and Θ_M, namely

$$B = \frac{6h^2}{mk_B}\frac{T}{\Theta_M^2}\left[\frac{T}{\Theta_M}\int_0^{\Theta_M/T}\frac{x\,dx}{(e^x-1)} + \frac{1}{4}\frac{\Theta_M}{T}\right], \quad (3)$$

in a standard notation (*e.g.* Willis & Pryor, 1975). Fig. 1 shows the resulting Θ_M deduced from (3). A comparison with the Debye temperature Θ_C derived from specific-heat data (as shown, for example, by Zdetsis & Wang, 1979) emphasizes that Θ_M is different from Θ_C in both magnitude and temperature dependence and provides a good warning against a confusion of these two quantities. It is possible, nevertheless, to deduce Θ_M from purely thermodynamic data and Fig. 1 includes the result of a Padé approximant analysis of thermodynamic results for silicon by Salter (1965). The agreement in both magnitude and general shape is encouraging.

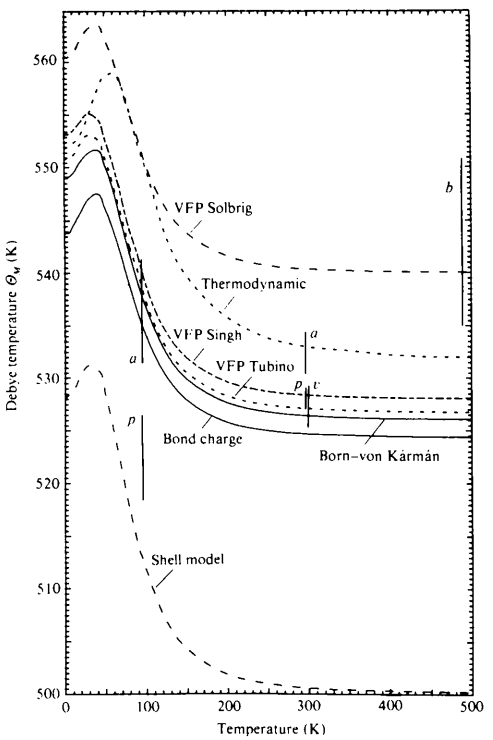

Fig. 1. The calculated Debye temperatures Θ_M for silicon given by the different lattice-dynamical models referenced in the text. The curve labelled 'thermodynamic' was derived by Salter (1965). The direct experimental results shown as bars come from: (*a*) Aldred & Hart (1973); (*b*) Batterman & Chipman (1962); (*p*) Price, Maslen & Mair (1978); and (*v*) Voland *et al.* (1976).

Also included for comparison in Fig. 1 are some experimental Θ_M deduced from X-ray analyses. The interpretation of these results is not completely clear. Early results, not shown on the figure, have tended to be too high, perhaps due to inadequate corrections for systematic effects such as TDS. Voland, Deus & Schneider (1976) give nine references to earlier work and their own value of 527·5 ± 2 calculated from their B value at 300 K agrees well with that of 528·2 ± 1 given at 293·2 K by Price, Maslen & Mair (1978). This latter value arises out of a most detailed scattering-factor analysis of the accurate data of Aldred & Hart (1973) measured both at room temperature and at 92·2 K but it cannot be assumed to be the best figure available. Aldred & Hart in their original analysis took care to deduce their values only from high-index reflections to ensure they referred only to motion of the core. Their values differ from those of Price and co-workers, as Fig. 1 shows, though unfortunately we cannot take the difference as giving a measure of the effect of the bonding electrons because this effect is likely to be masked by systematic differences introduced by the different charge-density model treatment of Price and co-workers.

The additional B values quoted in Table 1 and Fig. 1 are given by two models that do include dynamic deformation and which we shall be considering in the subsequent sections. The shell model is well known and for all the calculations in this paper we have used the program of Kunc & Nielsen (1979) for the 14-parameter model, with input data obtained from references listed with the tables. Dolling's (1963) shell model II*C* for silicon has in the past been extensively quoted and a calculation of its Debye–Waller B values reported in an earlier paper by Robertson & Reid (1979). The more recent bond-charge model of Weber (1977) appears to have much to recommend it and although it has only four disposable parameters its B values are not far from recent experimental values. There may even be scope for improvement if the model parameters are least-squares-fitted to all the experimental frequency data available.

A detailed analysis as to which model best represents the lattice frequencies of silicon (or the other three materials to be presented) is beyond the scope of this paper. However, the physical basis and suitability of the various models are discussed in all the source references containing the model parameters. It must also be mentioned that we have not covered *all* the good lattice-dynamical models suitable for silicon.

Finally, Table 2 shows Debye–Waller B values

Table 2. *Debye–Waller B values* (Å^2) *for diamond, germanium and α-tin*

The various models were generally fitted at room temperature for diamond, 100 K for germanium and 90 K for α-tin. The sampling of the Brillouin zone for the summations was usually the same as for the corresponding models for silicon. For the deformable atom models the sum of (1) was taken over 48 000 frequencies which can produce values up to about 0·2% too small at the higher temperatures, due in part to approximations in the treatment of the zero-phonon region.

	Diamond			Germanium				α-Tin		
Temperature (K)	Valence force[a]	Shell model[b]	Bond charge[d]	Valence force[a]	Born–von Kármán[e]	Shell model[b]	Bond charge[d]	Valence force[a]	Shell model[c]	Bond charge[d]
1·0	0·1283	0·1282	0·1277	0·1244	0·1262	0·1323	0·1282	0·1240	0·1374	0·1283
5·0	0·1283	0·1282	0·1277	0·1245	0·1263	0·1324	0·1282	0·1243	0·1377	0·1285
10·0	0·1283	0·1282	0·1277	0·1249	0·1269	0·1328	0·1286	0·1257	0·1394	0·1297
20·0	0·1284	0·1282	0·1278	0·1269	0·1295	0·1352	0·1307	0·1340	0·1523	0·1383
40·0	0·1286	0·1284	0·1279	0·1384	0·1434	0·1505	0·1434	0·1690	0·2022	0·1752
60·0	0·1289	0·1286	0·1282	0·1579	0·1658	0·1753	0·1648	0·2149	0·2644	0·2238
80·0	0·1293	0·1290	0·1286	0·1819	0·1928	0·2051	0·1910	0·2657	0·3315	0·2773
100·0	0·1299	0·1296	0·1291	0·2087	0·2224	0·2377	0·2200	0·3192	0·4013	0·3336
150·0	0·1320	0·1316	0·1312	0·2825	0·3032	0·3259	0·2994	0·4583	0·5815	0·4798
200·0	0·1354	0·1349	0·1344	0·3611	0·3888	0·4191	0·3837	0·6010	0·7653	0·6297
250·0	0·1400	0·1394	0·1389	0·4420	0·4767	0·5145	0·4703	0·7454	0·9507	0·7812
295·0*	0·1451	0·1445	0·1439	0·5160	0·5568	0·6015	0·5493	0·8325	1·0624	0·8726
350·0	0·1525	0·1519	0·1511	0·6072	0·6557	0·7087	0·6468			
400·0	0·1601	0·1595	0·1586	0·6906	0·7461	0·8067	0·7359			
500·0	0·1776	0·1768	0·1757	0·8584	0·9277	1·0035	0·9150			
600·0	0·1971	0·1962	0·1949	1·0269	1·1101	1·2009	1·0948			
700·0	0·2182	0·2171	0·2155	1·1958	1·2928	1·3989	1·2750			
800·0	0·2403	0·2391	0·2373	1·3650	1·4759	1·5970	1·4555			
900·0	0·2631	0·2618	0·2598	1·5343	1·6590	1·7953	1·6361			
1000·0	0·2866	0·2851	0·2828	1·7038	1·8423	1·9938	1·8168			

Notes: (*a*) Tubino *et al.* (1972). All the tables in this reference contain erroneous information though the authors' dispersion relations are correct. We are grateful to Dr L. Piseri who guided us to the correct matrix elements for the model. (*b*) Dolling & Cowley (1966), and Warren, Yarnell, Dolling & Cowley (1967). The parameter δ_R had to be taken as one quarter the published value for diamond to reproduce the dispersion curves. This may represent a mistake in the quoted units for δ_R. (*c*) Price, Rowe & Nicklow (1971). (*d*) Weber (1977). (*e*) Model (I) of Herman (1959). This model is a reasonable fit and does not use so many neighbours as the model of Zdetsis & Wang (1979).

* The α-tin values near room temperature are evaluated at 280 and not 295 K because of the phase transition at approximately 286 K.

calculated with some corresponding models for diamond, germanium and grey tin. As far as the authors are aware, they represent the best theoretical values available at present and should provide a good comparison for experimental results. It is immediately noticeable that the shell model gives larger B values than the other models except in the case of diamond. A comparison between the experimentally determined frequencies and the dispersion curves given in the source articles shows regions of significant difference, with the shell model tending to produce frequencies that are too low. It is likely that this fitting error is the major source of the deviation of B values, possibly reflecting the fact that the constraints placed on the general shell model to reduce the number of parameters to fourteen are not completely satisfactory for the Group IV elements. Although there are other appreciable and interesting differences shown by different models for one material, the range is typically much smaller than that displayed by experimental determinations. Indeed, there can be few quantities so apparently straightforward to determine as the Debye–Waller factor but in practice so elusive. Two aspects of the problem are well illustrated for diamond by the detailed work of Stewart (1973) and Price, Maslen & Moore (1978).

Dynamic deformation and the shell model

There are two ways of looking at an atom which is divided into subunits that can move relative to each other. Either the subunits can be treated as separate (but linked) quantities and each ascribed a Debye–Waller factor of its own, or the atom as a whole can be assigned an effective Debye–Waller factor which, through the coupling of the rest of the lattice to the deformation, will vary as the scattering vector **K**. After an elegant set of experiments measuring the 222 reflection of silicon, Fujimoto (1974) followed the first approach and tried to explain his results with the help of a calculation of the Debye–Waller factor of the shell in Dolling's shell model. In the absence of facilities to calculate the model eigendata he was unable to obtain a reliable result. The B values he was seeking are shown in Column 3 of Table 3 which was calculated by

evaluating the shell eigenvectors and the model frequencies in a sum over 48 000 phonon states in the Brillouin zone.

If these values for silicon are compared with any column of Table 1, and if it is remembered that B is directly proportional to the mean-square vibrational amplitude, it is clear that the shells vibrate substantially less than the cores, contrary to the suspicions of Fujimoto but in broad agreement with the behaviour of all the alkali-halide shells investigated in (I). For confirmation of the reasonableness of this result one looks to experimental determinations of the B values associated with the bonding electrons. However, a summary by Price, Maslen & Mair (1978) of fairly recent experimental results suggests disagreement amongst different investigations. The argument has been repeated several times that if the bonding electrons remain midway between neighbouring atoms which vibrate independently then the B value for the bonds would be expected to be 0·5 that of the cores. If one identifies the shell with some average property of the bonding electrons, then the shell model indicates that the bonds vibrate slightly less than this, forming a moderately rigid structure within which the cores move. In silicon, the core–shell force constant is fairly weak and one can imagine that as the cores drive the shells through this soft spring against the reaction of Coulomb forces and nearest-neighbour forces the shells fail to move as much as the cores causing the atom to appreciably dynamically deform. Table 3 also shows that there is a similar effect in germanium. With diamond and grey tin the shell–core force constant is several times larger and, with a larger shell charge, this suggests that there is a fairly rigid coupling between core and shell and hence B values for the shell are comparable to those of the core.

Table 3. *Debye–Waller B values* (Å^2) *for the shells only, in the shell models for diamond, silicon, germanium and* α*-tin*

Temperature (K)	Diamond	Silicon	Germanium	α-Tin
1·0	0·0974	0·0763	0·0375	0·0941
5·0	0·0975	0·0763	0·0376	0·0944
10·0	0·0975	0·0765	0·0379	0·0958
20·0	0·0975	0·0772	0·0395	0·1048
40·0	0·0976	0·0806	0·0456	0·1378
60·0	0·0979	0·0867	0·0541	0·1784
80·0	0·0983	0·0948	0·0638	0·2224
100·0	0·0988	0·1041	0·0743	0·2683
150·0	0·1007	0·1309	0·1024	0·3872
200·0	0·1035	0·1606	0·1320	0·5087
250·0	0·1072	0·1919	0·1622	0·6315
295·0*	0·1114	0·2210	0·1897	0·7054
350·0	0·1172	0·2573	0·2236	
400·0	0·1233	0·2908	0·2545	
500·0	0·1369	0·3585	0·3167	
600·0	0·1522	0·4269	0·3791	
700·0	0·1685	0·4958	0·4416	
800·0	0·1857	0·5649	0·5042	
900·0	0·2034	0·6341	0·5668	
1000·0	0·2216	0·7035	0·6295	

* The α-tin value near room temperature is evaluated at 280 and not 295 K.

The alternative approach of treating the deforming atom as a whole is worth studying because it may not be known during a general analysis whether a particular atom is (or is not) deforming significantly. It has been shown in (I) that the Debye–Waller exponent W_k^D of a deforming atom consists of the normal exponent W_k plus a **K**-dependent modification ΔW_k, *i.e.*

$$W_k^D = W_k + \Delta W_k,$$

where, in a conventional notation detailed in (I),

$$\Delta W_k = -i \sum_{\lambda} (2n_\lambda + 1)\beta(k/\lambda)K^*(k/\lambda). \tag{4}$$

Although this expression holds good for the alkali halides it is important to examine its validity for the less symmetric silicon structure since its derivation in (I) ultimately used a transformation law for $\beta(l',kk',\mathbf{K})$ given by Reid (1974) which does not have the necessary generality.

Let the symmetry operator $\{T/\mathbf{V}(T) + \mathbf{r}(m)\}$ acting on site coordinate $\mathbf{r}(l'k')$ transform it to $\mathbf{r}(l'_T k'_T)$ and the origin site $\mathbf{r}(0k)$ to $\mathbf{r}(0k_T)$. Then, if the equilibrium scattering factors are taken as spherically symmetric, which is usually the case, the transformation of the real-space β parameter obeys

$$\beta(l'_T,k_Tk'_T,\mathbf{K}) = \beta(l',kk',\mathbf{K}T)\tilde{T}. \tag{5}$$

As far as inversion is concerned, this relation no longer provides any general requirements of evenness or oddness of β because it now relates parameters on different sites. However, the simplifying transformations for the $\beta(k/\lambda)$, which affect the Debye–Waller factor, remain true in full generality, though they are now associated with whether $\beta(l',kk',\mathbf{K})$ is real or imaginary. In particular,

$$\beta(k/-\lambda) = \mp\beta^*(k/\lambda) \begin{cases} - \text{ sign for real } \beta(l',kk',\mathbf{K}) \\ + \text{ sign for imaginary } \beta(l',kk',\mathbf{K}). \end{cases} \tag{6}$$

If (6) is applied to the effect of dynamic deformation on the Debye–Waller factor it is straightforward to see that there will be no effect for all deformation processes which give a real $\beta(l',kk',\mathbf{K})$ and a finite effect given by (4) for those processes which give imaginary $\beta(l',kk',\mathbf{K})$.

The shell model, without breathing, gives imaginary $\beta(l',kk',\mathbf{K})$. If the deformation is modelled by an isotropic shell, then ΔW_k depends only on the magnitude of **K** through the ratio of shell-to-atom scattering factors. Because of the complex eigen-

vectors introduced by the non-symmorphic silicon structure, the expression for the equivalent ΔB_k does not simplify to quite the same form as with the alkali halides but becomes

$$\Delta B_k = \frac{[f(\mathbf{K})]_{\text{shell}}}{[f(\mathbf{K})]_{\text{atom}}} \frac{8\pi^2}{3N} \sum_{\lambda} \left(\frac{E}{\omega^2}\right)_{\lambda} \times \left[\mathscr{W}(\mathrm{k}/\lambda). \frac{\mathscr{E}^*(k/\lambda)}{m_k^{1/2}} + \mathscr{W}^*(k/\lambda). \frac{\mathscr{E}(k/\lambda)}{m_k^{1/2}} \right], \quad (7)$$

where $\mathscr{W}(k/\lambda)$ is the complex relative shell-core displacement; *i.e.*

$$\Delta B = \frac{[f(\mathbf{K})]_{\text{shell}}}{[f(\mathbf{K})]_{\text{atom}}} S, \quad (8)$$

defining the constant S determined by the lattice dynamics of the model. The atom type suffix k can be dropped in the silicon structure because of the identity of the atoms in the two sites.

Summing over a mesh of 8000 wavevectors uniformly covering the Brillouin zone gives the S values shown in Table 4. Fig. 2(*a*) shows the kind of behaviour expected for $\Delta B/B$ when estimates are made of the ratio of shell/atom scattering factors based on the data in *International Tables for X-ray Crystallography* (1974) and partial scattering factors published by James & Brindley (1931). The broken curves are those obtained when $[f(\mathbf{K})]_{\text{shell}}$ is taken as the scattering factor of a single outer electron. The solid lines show the total prediction of the shell model obtained by scaling the single-electron results by the model shell charge. [The shell charge also affects S so the two components in (8) are not as independent for the shell model as they may at first seem.] Of course, the impossibility of physically identifying the shell means that Fig. 2(*a*) is more of a guide to the expected behaviour than a positive assertion. Nevertheless, the effect should be observable at lower sin θ/λ values even though the Debye–Waller factors themselves are quite small at room temperature. There is less of an uncertainty in the calculated temperature dependence of $\Delta B/B$ which does not require an estimate of the shell scattering factor, provided the nature of the shell itself is temperature independent. Fig. 2(*b*) shows the remarkable constancy of $\Delta B/B$ with temperature.

Table 4. *Values of S/B at* 295 K

This ratio, see (7) and (8), is the governing lattice-derived parameter determining the fractional effect of the dynamic deformation on the Debye–Waller factor.

	S/B
Diamond	−0·2568
Silicon	−0·7475
Germanium	−0·9692
α-Tin	−0·3834

The bond-charge model

The bond-charge dynamical model in which the valence electrons are distributed in bonds between neighbouring cores seems a most natural description of the silicon-type structure. Weber (1977) has discussed the merits of several such models and presented in detail his adiabatic bond-charge model in which the bond charges are allowed to move adiabatically under the balance of Coulomb forces and short-range bond–core

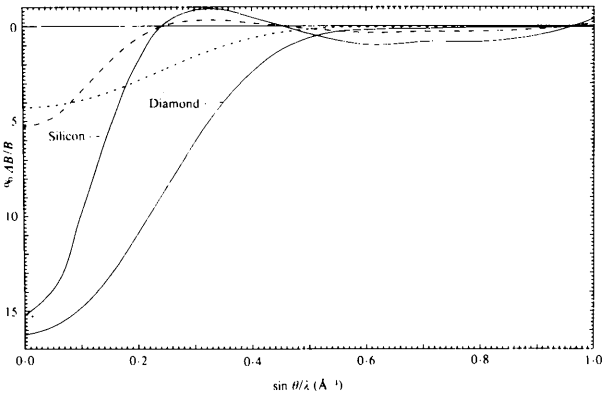

(*a*)

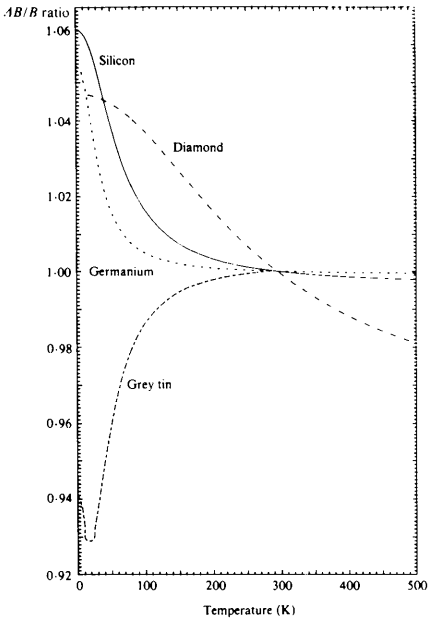

(*b*)

Fig. 2. Values for the fractional change in Debye–Waller B produced by the dynamic deformation given by the shell model. (*a*) An estimate of the effect as a function of sin θ/λ for diamond and silicon. The broken lines take a shell charge of one electron and the solid lines scale by the model shell charge of 2·87 e for silicon and 3·80 e for diamond. (*b*) The variation of $\Delta B/B$ with temperature relative to the value at room temperature for the four silicon-like elements.

and bond–bond forces. As Weber's model is probably the best such model we shall limit outselves to calculations based on his parameters.

Concerning the Debye–Waller factors of the bond charges, Price, Maslen & Mair (1978) have summarized some of the recent discussion in the literature. However, it has not been pointed out that even though bond charges midway between the cores are at sites of inversion symmetry, their Debye–Waller factors are necessarily anisotropic in the silicon structure. The general deformation formalism can cope with this situation provided equation (7) in (I) is modified to include a sum over the bond-charge scattering factors and eigenvectors, with the addition of appropriate phase factors required by the offset between the centres of the bond charges and the cores.

However, when the subunits of a deforming atom are in four parts extending halfway to the next atom it becomes less meaningful to consider the atom as a whole with an effective Debye–Waller factor and more reasonable to discuss directly the Debye–Waller factors of the bond charges themselves, since they can be seen as separate electron density units without requiring outstanding resolution.

If the bond charges are labelled as in Fig. 3, the anisotropic bond-charge Debye–Waller factor for the scattering vector **K** is

$$W(K) = C\,(K_x^2 + K_y^2 + K_z^2) + 2D \times \begin{cases} K_xK_y + K_yK_z + K_zK_x \text{ for bond charge 3} \\ K_xK_y - K_yK_z - K_zK_x \text{ for bond charge 4} \\ -K_xK_y - K_yK_z + K_zK_x \text{ for bond charge 5} \\ -K_xK_y + K_yK_z - K_zK_x \text{ for bond charge 6,} \end{cases} \quad (9)$$

where C and D are determined from the bond-charge eigenvectors (and, of course, the lattice frequencies and the temperature).

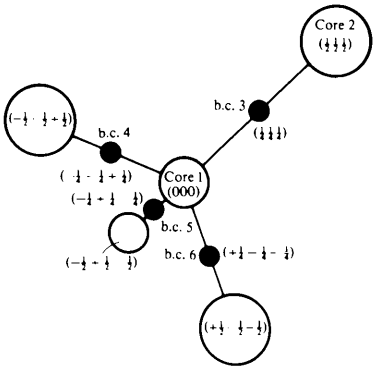

Fig. 3. Labelling of the bond charges (b.c.) in the silicon structure with coordinates shown in units of a, one half of the cubic cell side. The open circles for the cores and the black dots for the bond charges merely show location and are not representative of size or other detail of the corresponding electron distribution.

For the silicon structure, with eigenvectors that include the phase factor $\exp[i\mathbf{q}.\mathbf{r}(kk')]$ the general 18×1 displacement eigenvector for the bond-charge model can be written for any wavevector as:

$$\begin{pmatrix} \mathscr{E}(1) \\ \mathscr{E}^*(1) \\ \mathbf{V}(3) \\ \mathbf{V}(4) \\ \mathbf{V}(5) \\ \mathbf{V}(6) \end{pmatrix}, \quad (10)$$

where $\mathscr{E}(1)$ is the three-component complex eigenvector for the origin core, $\mathscr{E}^*(1)$ that for the second core and $\mathbf{V}(3) \rightarrow \mathbf{V}(6)$ are real three-component displacement eigenvectors for the bond charges labelled $k = 3, 4, 5$ and 6. The eighteen-component eigenvectors may not appear with this symmetry after diagonalizing the dynamical matrix but each one can be so transformed with the aid of an appropriate phase factor. The isotropic term C and the anisotropic term D may now be determined from the bond-charge eigenvectors after some reduction with the eigenvector symmetry transformations of Maradudin & Vosko (1968):

$$C = \frac{1}{2N}\frac{1}{12}\sum_{\lambda}\left(\frac{E}{\omega^2}\right)_{\lambda} \times \sum_{k=3}^{6}[V_x^2(k) + V_y^2(k) + V_z^2(k)] \quad (11)$$

and

$$\begin{aligned} D = \frac{1}{2N}\frac{1}{12}\sum_{\lambda}\left(\frac{E}{\omega^2}\right)_{\lambda} [&V_x(3)V_y(3) + V_x(3)V_z(3) \\ &+ V_y(3)V_z(3) + V_x(4)V_y(4) - V_x(4)V_z(4) \\ &- V_y(4)V_z(4) - V_x(5)V_y(5) + V_x(5)V_z(5) \\ &- V_y(5)V_z(5) - V_x(6)V_y(6) - V_x(6)V_z(6) \\ &+ V_y(6)V_z(6)]. \end{aligned} \quad (12)$$

Since both isotropic and anisotropic terms vary quadratically with **K**, the bond-charge Debye–Waller factor can be characterized in reciprocal space by a shape and a magnitude. With the bond charge along [111] as an example, the shape is cylindrically symmetrical about [111], as shown in Fig. 4. For **K** along [111], a B value can be generated from the relationship

$$\begin{aligned} W &= B\sin^2\theta/\lambda^2 \\ &= B_I(K_x^2 + K_y^2 + K_z^2)/16\,\pi^2 \\ &\quad + B_A(K_xK_y + K_yK_z + K_zK_x)/16\,\pi^2, \end{aligned}$$

giving

$$B_I = 16\,\pi^2\,C, \quad (13)$$

the isotropic B value, and

$$B_A = 16\,\pi^2 \times 2D, \quad (14)$$

Table 5. *Values for the isotropic and anisotropic components of the bond-charge Debye–Waller factors in* Å^2 *for diamond,* Si, Ge *and* α-Sn

In certain circumstances, explained in the text, these values can be meaningfully compared with the core values in Tables 1 and 2. Equations (11)–(14) relate the tabulated constants to the general anisotropic Debye–Waller exponent constants for the bond charges.

Temperature	Diamond		Silicon		Germanium		α-Tin	
(K)	B_I	B_A	B_I	B_A	B_I	B_A	B_I	B_A
1·0	0·0724	−0·0059	0·0917	−0·0275	0·0624	−0·0161	0·0637	−0·0086
5·0	0·0724	−0·0059	0·0917	−0·0275	0·0625	−0·0161	0·0639	−0·0086
10·0	0·0724	−0·0059	0·0919	−0·0275	0·0628	−0·0161	0·0649	−0·0087
20·0	0·0724	−0·0059	0·0926	−0·0275	0·0645	−0·0162	0·0702	−0·0096
40·0	0·0726	−0·0059	0·0962	−0·0278	0·0727	−0·0179	0·0903	−0·0129
60·0	0·0729	−0·0059	0·1029	−0·0290	0·0852	−0·0207	0·1160	−0·0170
80·0	0·0733	−0·0059	0·1121	−0·0309	0·1000	−0·0242	0·1441	−0·0213
100·0	0·0738	−0·0059	0·1230	−0·0333	0·1161	−0·0281	0·1735	−0·0258
150·0	0·0757	−0·0059	0·1548	−0·0408	0·1596	−0·0385	0·2499	−0·0374
200·0	0·0787	−0·0059	0·1902	−0·0495	0·2054	−0·0495	0·3281	−0·0492
250·0	0·0826	−0·0059	0·2277	−0·0587	0·2524	−0·0608	0·4072	−0·0611
295·0*	0·0868	−0·0060	0·2625	−0·0674	0·2951	−0·0711	0·4549	−0·0683
350·0	0·0927	−0·0061	0·3058	−0·0783	0·3478	−0·0838		
400·0	0·0986	−0·0062	0·3458	−0·0883	0·3959	−0·0954		
500·0	0·1117	−0·0065	0·4267	−0·1087	0·4926	−0·1186		
600·0	0·1261	−0·0069	0·5083	−0·1293	0·5896	−0·1420		
700·0	0·1412	−0·0074	0·5904	−0·1500	0·6868	−0·1654		
800·0	0·1569	−0·0080	0·6728	−0·1709	0·7841	−0·1888		
900·0	0·1730	−0·0086	0·7554	−0·1917	0·8815	−0·2123		
1000·0	0·1894	−0·0092	0·8381	−0·2127	0·9789	−0·2358		

* As with Table 2, the α-tin values near room temperature are evaluated at 280 and not 295 K because of the phase transition at approximately 286 K.

which is a suitable single parameter for the anisotropic component of B. Since C and D are themselves small quantities, Table 5 shows values for B_I and B_A which, with the shape of Fig. 4 in mind, lend themselves to a direct comparison with the core Debye–Waller B values of Table 1.

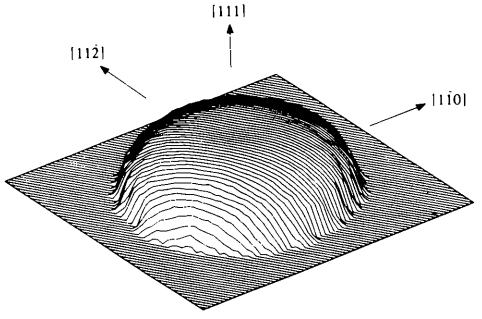

Fig. 4. The shape of the anisotropic bond-charge Debye–Waller exponent $W(\mathbf{K})$ in reciprocal space for the bond charge at $(\frac{1}{4}\frac{1}{4}\frac{1}{4})a$. $W(\mathbf{K})$ has been evaluated over a sphere of constant K^2 and is represented for each $\mathbf{K}$ by a vector of length $W(\mathbf{K})$ extending from the origin in the direction of $\mathbf{K}$. The figure shows half the resulting surface, cut by a diametral plane, and has been drawn from the low-temperature data for silicon which gives a very slight dip along the [111] direction, just discernible in the figure. With greater anisotropy the dip becomes pronounced but, in fact, the anisotropy decreases with increasing temperature by an amount sufficient to remove the dip. The shape is cylindrically symmetric about the [111] axis, small irregularities in the diagram merely reflecting small approximations made by the drawing algorithm. The magnitude of $W(\mathbf{K})$ in any direction scales as K^2.

In real space, the mean-square vibrational ellipsoids for the bond charges are oblate spheroids with the minor axis lying along the line between the neighbouring cores. Taking silicon at room temperature as an example, the 50% probability surface (Nelmes, 1969) has a semi-minor axis of 0·0659 Å along [111] and equal semi-major axes of 0·0859 Å along [1$\bar{1}$0] and [11$\bar{2}$], compared with the core 50% probability sphere of radius 0·119 Å. Ellipsoid sizes for the other materials (and temperatures) can be calculated from the data in Table 5 following the method discussed by Willis & Pryor (1975).

Conclusions

An erroneous treatment of the Debye–Waller factors during a structure analysis may cause errors to propagate to the mean atomic site coordinates, or, through the scattering factors, to the charge density if it too is being determined. Dynamic deformation will influence the Debye–Waller factors in a different way from anharmonicity since only the smaller values of sin θ/λ will be affected. It is just in this region, however, that the strongest reflections tend to occur and hence one is led to feel that there is some physical justification for allowing an additional fitting parameter $\Delta B_k(K)$ for these reflections. After fitting, an examination of the variation ΔB_k with scattering vector

K can determine whether its behaviour could reasonably arise from dynamic deformation. Thus, in principle, accurate X-ray powder data from suitable materials could be used to investigate the effect of dynamic deformation provided absorption, extinction, TDS and other systematic effects can be evaluated accurately. However, it must be added that the Group IV elements are not ideal experimental subjects because most of the Bragg reflections occur at too high values of sin θ/λ due to systematic absences and small lattice constants.

Although the fractional effect of dynamic deformation is fairly temperature independent, the increasing importance of the Debye–Waller B values with temperature implies that neglect of the effect may contribute to poorer fits at high temperatures than at low temperatures. In addition, the absence of the effect in neutron scattering (and in Mössbauer absorption studies, for example on ^{119}Sn) could provide a means of experimentally determining the effect if all other factors are adequately known. It also means that care must be taken when interpreting neutron and X-ray data given by the same material. At a simple level, some of the discrepancies found between X-ray and nuclear Debye–Waller B values may be contributed by dynamic deformation. Certainly the calculations presented here have shown that even for the tightly bonded diamond-like elements dynamic-deformation effects are significant.

The anisotropic bond-charge B values are possibly the first such values to be calculated from a lattice-dynamical model. It would be interesting to ascertain experimentally whether the model adequately describes the situation. It does seem certain that the B values for the bonding electrons are very different from those of the core electrons and that this must be seriously considered in accurate bond-charge determinations.

We appreciate the help of Ronald Yorston in preparing Figs. 1 and 4. We are grateful for the generous use of the Honeywell 66/80 computer at Aberdeen University, for the use of the graphics package *SYMVU* made available by courtesy of Harvard University and for grant support by the Science Research Council.

References

ALDRED, P. J. E. & HART, M. (1973). *Proc. R. Soc. London Ser. A*, **332**, 239–254.

BATTERMAN, B. W. & CHIPMAN, D. R. (1962). *Phys. Rev.* **127**, 690–693.

BORN, M. (1942). *Proc. R. Soc. London Ser. A*, **180**, 397–413.

BUYERS, W. J. L., PIRIE, J. D. & SMITH, T. (1968). *Phys. Rev.* **165**, 999–1005.

DOLLING, G. (1963). *Inelastic Scattering of Neutrons in Solids and Liquids*, pp. 37–47. Vienna: IAEA.

DOLLING, G. & COWLEY, R. A. (1966). *Proc. Phys. Soc. London*, **88**, 463–494.

FUJIMOTO, I. (1974). *Phys. Rev. B*, **9**, 591–599.

HERMAN, F. (1959). *J. Phys. Chem. Solids*, **8**, 405–418.

International Tables for X-ray Crystallography (1974). Vol. IV. Birmingham: Kynoch Press.

JAMES, R. W. & BRINDLEY, G. W. (1931). *Philos. Mag.* **12**, 81–112.

KUNC, K. & NIELSEN, O. H. (1979). *Comput. Phys. Commun.* **17**, 413–422.

MARADUDIN, A. A. & VOSKO, S. H. (1968). *Rev. Mod. Phys.* **40**, 1–8.

NELMES, R. J. (1969). *Acta Cryst.* A**25**, 523–526.

PRICE, D. L., ROWE, J. M. & NICKLOW, R. M. (1971). *Phys. Rev. B*, **3**, 1268–1279.

PRICE, P. F., MASLEN, E. N. & MAIR, S. L. (1978). *Acta Cryst.* A**34**, 183–193.

PRICE, P. F., MASLEN, E. N. & MOORE, F. H. (1978). *Acta Cryst.* A**34**, 171–172.

REID, J. S. (1974). *J. Phys. C*, **7**, 3444–3452.

REID, J. S. (1979). *Acta Cryst.* A**35**, 445–448.

ROBERTSON, B. F. & REID, J. S. (1979). *Acta Cryst.* A**35**, 785–788.

SALTER, L. S. (1965). *Adv. Phys.* **14**, 1–37.

SINGH, B. D. & DAYAL, B. (1970). *Phys. Status Solidi*, **38**, 141–150.

SOLBRIG, A. W. (1971). *J. Phys. Chem. Solids*, **32**, 1761–1768.

STEWART, R. F. (1973). *Acta Cryst.* A**29**, 602–605.

TUBINO, R., PISERI, L. & ZERBI, G. (1972). *J. Chem. Phys.* **56**, 1022–1039.

VOLAND, U., DEUS, P. & SCHNEIDER, H. A. (1976). *Phys. Status Solidi A*, **36**, K165–K169.

WARREN, J. L., YARNELL, J. L., DOLLING, G. & COWLEY, R. A. (1967). *Phys. Rev.* **158**, 805–808.

WEBER, W. (1977). *Phys. Rev. B*, **15**, 4789–4803.

WILLIS, B. T. M. & PRYOR, A. W. (1975). *Thermal Vibrations in Crystallography*. Cambridge Univ. Press.

ZDETSIS, A. D. & WANG, C. S. (1979). *Phys. Rev. B*, **19**, 2999–3003.